Tolerogenic nanoparticles suppress central nervous system inflammation

Jessica E. Kenison[a,b], Aditi Jhaveri[c], Zhaorong Li[d], Nikita Khadse[c], Emily Tjon[d], Sara Tezza[c], Dominika Nowakowska[c], Agustin Plasencia[c], Vincent P. Stanton Jr[c], David H. Sherr[a,b], and Francisco J. Quintana[d,e,1]

[a]Department of Pathology, Boston University School of Medicine, Boston, MA 02118; [b]Department of Environmental Health, Boston University School of Public Health, Boston, MA 02118; [c]AnTolRx, Inc., Cambridge, MA 02139; [d]Ann Romney Center for Neurologic Diseases, Brigham and Women's Hospital, Harvard University Medical School, Boston, MA 02115; and [e]Broad Institute of Massachusetts Institute of Technology and Harvard University, Cambridge, MA 02142

Edited by Lawrence Steinman, Stanford University School of Medicine, Stanford, CA, and approved October 6, 2020 (received for review August 4, 2020)

Therapeutic approaches for the induction of immune tolerance remain an unmet clinical need for the treatment of autoimmune diseases, including multiple sclerosis (MS). Based on its role in the control of the immune response, the ligand-activated transcription factor aryl hydrocarbon receptor (AhR) is a candidate target for novel immunotherapies. Here, we report the development of AhR-activating nanoliposomes (NLPs) to induce antigen-specific tolerance. NLPs loaded with the AhR agonist ITE and a T cell epitope from myelin oligodendrocyte glycoprotein (MOG)$_{35–55}$ induced tolerogenic dendritic cells and suppressed the development of experimental autoimmune encephalomyelitis (EAE), a preclinical model of MS, in preventive and therapeutic setups. EAE suppression was associated with the expansion of MOG$_{35–55}$-specific FoxP3$^+$ regulatory T cells (Treg cells) and type 1 regulatory T cells (Tr1 cells), concomitant with a reduction in central nervous system-infiltrating effector T cells (Teff cells). Notably, NLPs induced bystander suppression in the EAE model established in C57BL/6 × SJL F1 mice. Moreover, NLPs ameliorated chronic progressive EAE in nonobese diabetic mice, a model which resembles some aspects of secondary progressive MS. In summary, these studies describe a platform for the therapeutic induction of antigen-specific tolerance in autoimmune diseases.

EAE | MS | autoimmunity | nanoparticles | antigen-specific therapy

Autoimmune diseases are driven by dysregulated adaptive immunity against self-antigens. Current approaches for the treatment of autoimmune diseases rely on nonspecific immunosuppression, and are associated with adverse side effects. Thus, there is an unmet clinical need for therapies that reestablish immune tolerance in an antigen-specific manner (1).

Multiple mechanisms enforce immunologic tolerance. Mechanisms of central tolerance eliminate self-reactive lymphocytes in the thymus and bone marrow, but do not remove all of the autoreactive T cells and B cells (2, 3). However, additional immunoregulatory mechanisms are in place to prevent the development of pathogenic autoimmunity. Among these additional mechanisms are specialized thymic-derived regulatory FoxP3$^+$ T cells (natural Tregs, nTregs) and peripherally induced regulatory cells which include FoxP3$^+$ Tregs as well as IL-10$^+$ type 1 regulatory cells (Tr1 cells) (4–6). Autoimmune diseases have been linked to reduced numbers, function, and stability of multiple regulatory T cell populations, and/or the resistance of effector T cells to Treg modulation (7). Thus, the expansion of the Treg compartment is a potential approach for the treatment of autoimmunity (8).

The aryl hydrocarbon receptor (AhR) is a ligand-activated transcription factor with important roles in the control of the immune response (9–11). AhR signaling can modulate the differentiation of T cell subsets (12–15) as well as the function of antigen presenting cells (APCs), including dendritic cells (DCs) and macrophages (16, 17). Indeed, we and others showed that AhR controls the differentiation of DCs and their ability to activate and polarize regulatory T (Treg) and effector T (Teff) cells (16, 18–22). In support of the potential therapeutic relevance of these observations, AhR activation with natural or synthetic ligands ameliorates disease in preclinical models of multiple sclerosis (MS) (15, 16), type 1 diabetes (23), and inflammatory bowel disease (14, 24), among others, suggesting that AhR is a potential target for the therapeutic reestablishment of antigen-specific tolerance in autoimmune diseases.

Nanomaterials, including nanoparticles and nanoliposomes (NLPs), provide novel opportunities to overcome the limitations associated with immunosuppressive drugs currently in use (25). Nanoparticles and NLPs can be used as platforms to deliver drugs of interest to target APCs while protecting these drugs from degradation and clearance. Indeed, NLPs are already in use for the delivery of the Food and Drug Administration (FDA)-approved therapeutic agents, with well-characterized safety and tolerability profiles (26, 27). Here, we report the use of NLPs to codeliver the tolerogenic AhR ligand 2-(1′H-indole-3′-carbonyl)-thiazole-4-carboxylic acid methyl ester (ITE) and a T cell epitope from myelin oligodendrocyte protein (MOG$_{35–55}$). ITE and MOG$_{35–55}$ coadministration via NLPs modulated myelin-specific T cells and suppressed disease development in mouse preclinical models of relapsing-remitting and secondary progressive MS. In summary, we describe an NLP-based platform for the induction of antigen-specific tolerance in autoimmune diseases.

Results

Characterization of the Transcriptional Response of DCs to AhR Activation by ITE. DCs, as well as other APCs, control T cell activation and polarization in vivo (28–31). AhR signaling modulates the ability of

Significance

Current treatments for autoimmune diseases rely on nonspecific immunosuppression, risking important complications and limiting the long-term use of these approaches for the treatment of chronic human autoimmunity. Thus, there is an unmet need for therapeutic approaches to reestablish immune tolerance in autoimmune disorders in an antigen-specific manner. Here, we describe a nanoliposome (NLP)-based platform for the induction of antigen-specific tolerance via the modulation of signaling by the aryl hydrocarbon receptor. These NLPs suppress disease pathology and pathogenic autoimmunity in preclinical models of multiple sclerosis, providing a candidate antigen-specific therapeutic approach for the management of autoimmune disorders.

Author contributions: J.E.K., A.J., S.T., D.N., A.P., V.P.S., D.H.S., and F.J.Q. designed research; J.E.K., A.J., N.K., S.T., D.N., and A.P. performed research; A.J. and N.K. contributed new reagents/analytic tools; J.E.K., A.J., Z.L., E.T., S.T., D.N., A.P., V.P.S., D.H.S., and F.J.Q. analyzed data; and J.E.K., D.H.S., and F.J.Q. wrote the paper.

Competing interest statement: J.E.K, A.J., N.K., S.T., D.N., A.P., V.P.S. are/were employees at AnTolRx; F.J.Q. is a consultant at AnTolRx. This work was partially funded by AnTolRx.

This article is a PNAS Direct Submission.

Published under the PNAS license.

[1]To whom correspondence may be addressed. Email: fquintana@rics.bwh.harvard.edu.

First published November 25, 2020.

Downloaded at Palestinian Territory, occupied on November 30, 2021

www.manaraa.com

DCs to control T cell responses (16, 20–22). However, little is known about the kinetics of AhR-driven transcriptional programs in DCs. To address this point, we first analyzed the effect of AhR activation in human DCs on the expression of the AhR transcriptional target genes *CYP1A1* and *CYP1B1* (32). We found that the mucosa-associated AhR agonist ITE (33) induced maximal *CYP1A1* and *CYP1B1* expression at a dose similar to the prototypical AhR agonist, 2,3,7,8-tetrachlorodibenzo-p-dioxin (TCDD) (Fig. 1*A*, *CYP1A1* effective concentration $[EC]_{50ITE}$ = 8.101 nM, EC_{50TCDD} = 4.166 nM; *CYP1B1* EC_{50ITE} = 1.462 nM, EC_{50TCDD} = 2.178 nM). Indeed, both ITE and TCDD induced *CYP1A1* and *CYP1B1* expression at concentrations 3 to 4 log folds lower than other AhR agonists such as laquinimod (Laq) (34), indoxyl-3-sulfate (I3S), and L-kynurenine (Kyn) (Fig. 1*A*, *CYP1A1* EC_{50Laq} = 9.117 μM, EC_{50I3S} = 47.781 μM, EC_{50Kyn} = 236.711 μM; *CYP1B1* EC_{50Laq} = 2.783 μM, EC_{50I3S} = 19.322 μM, EC_{50Kyn} = 47.249 μM). While *CYP1A1* expression showed an early peak followed by a return to baseline (Fig. 1*B*), the expression of *IDO1* and *IDO2*, which encode immunosuppressive enzymes involved in tryptophan catabolism (35), peaked early on and remained above baseline over the next 48 h. These data suggest that different transcriptional modules characterize the early, intermediate, and late responses to AhR activation in DCs.

To further investigate the kinetics of the AhR-driven transcriptional response, we treated peripheral DCs from three healthy donors with ITE for 6, 18, or 72 h, and performed RNA sequencing (RNA-seq) to identify gene signatures associated with early, intermediate, and late responses to AhR activation. We found that the number of genes differentially regulated in response to AhR activation with ITE was decreased over time (714 genes at 6 h, 624 genes at 18 h, and 468 genes at 72 h) (Fig. 1*C*). The analysis of 12 genes known to be regulated by AhR (16, 17, 20, 29, 36, 37) showed that the expression of most of these genes was up-regulated at the early timepoint (6 h) but decreased by 72 h; a small gene subset including *ALDH1A1*, *ALDH1A2*, and *IL10* was only up-regulated at intermediate or late timepoints (Fig. 1*D*).

Gene set enrichment analysis determined that genes associated with the regulation of the innate immune response, the response to type 1 interferons and other cytokines were significantly altered over time (Fig. 1*E*). Genes whose expression was regulated by AhR activation in "early" (6 h) transcriptional modules were associated with the down-regulation of signaling pathways, including IL-23, CD40, and NF-κB (Fig. 1*F*). AhR-driven "intermediate" (18 h) transcriptional modules were associated with the promotion of T cell exhaustion and PD-1/PD-L1 signaling (Fig. 1*F*). AhR-driven "late" (72 h) transcriptional modules were associated with down-regulation of EGF and leukocyte extravasation signaling (Fig. 1*F*).

Since differences in agonistic activity have been reported between human and mouse AhR (38–41), we investigated the similarity of the transcriptional response of human and murine DCs to stimulation with ITE. First, we compared the ability of ITE to activate AhR in mouse and human DCs by comparing the expression of the AhR transcriptional target genes *Cyp1a1* and *Cyp1b1*. ITE induced maximal *Cyp1a1* and *Cyp1b1* expression at similar doses in both species (Fig. 2*A*, human *CYP1A1* EC_{50ITE} = 6.701 nM, murine *Cyp1a1* EC_{50ITE} = 2.228 nM; human *CYP1B1* EC_{50ITE} = 1.958 nM, murine *Cyp1b1* EC_{50ITE} = 1.103 nM). Of note, the expression of *Ido1* and *Ido2* was strongly induced in murine ITE-stimulated DCs (Fig. 2*B*, *Ido1* EC_{50ITE} = 0.757 nM, *Ido2* EC_{50ITE} = 0.573 nM). Furthermore, ITE induced early, intermediate, and late responses in murine DCs, with *Cyp1a1* induction showing an early peak, followed by a return to baseline (Fig. 2*C*), while the expression of *Ido1* and *Ido2* was up-regulated over a more prolonged period of time. Interestingly, in murine DCs, *Cyp1b1* induction was highest both at the early timepoint and then again at the late timepoint (Fig. 2*C*).

To further investigate the kinetics of the AhR-driven transcriptional response in mice, we treated splenic DCs isolated from three separate pools of 10 mice with ITE for 6, 18, or 72 h, and performed RNA sequencing. We found that, similar to what was observed in human DCs, the number of genes differentially regulated by ITE decreased over time (595 genes at 6 h, 512 genes at 18 h, and 290 genes at 72 h) (Fig. 2*D*). The analysis of known AhR-regulated genes showed that the expression of most genes was up-regulated at the early timepoint (6 h) and decreased by 72 h, a small subset of genes was up-regulated at both the early and late timepoints, while another small gene subset was only up-regulated at intermediate or late timepoints (Fig. 2*E*).

Gene set enrichment analysis determined that genes associated with regulation of the innate immune response, response to type 1 IFN, and cytokine stimuli were significantly altered over time (Fig. 2*F*), similar to what was observed in human DCs. AhR-driven early (6 h) transcriptional modules were associated with the suppression of DC maturation and IFN signaling and the promotion of PD-1/PD-L1 signaling (Fig. 2*G*). AhR-driven "mid" (18 h) transcriptional modules were associated with the down-regulation of IL-15 and NF-κB signaling (Fig. 2*G*). AhR-driven late (72 h) transcriptional modules were associated with down-regulation of PPARα signaling and the promotion of cAMP-mediated signaling (Fig. 2*G*). Collectively, these results suggest that AhR activation by ITE in mouse and human DCs induces transcriptional responses associated with the induction of immunoregulatory/immunosuppressive mechanisms.

Generation of NLPs Loaded with $MOG_{35–55}$ and the Tolerogenic AhR Ligand ITE. AhR activation by ITE induces a tolerogenic phenotype in DCs which promotes the differentiation of regulatory T cells (16, 21, 22). We have shown that gold nanoparticles loaded with ITE and disease-specific antigens induce tolerance in models of autoimmunity (21, 22). NLPs present several advantages over gold nanoparticles, including ease of manufacturing and scalability, fine control of small molecule and antigen loading, and well-characterized safety and tolerability based on FDA-approved therapeutics (26, 27). Thus, we explored the potential of NLPs loaded with ITE and $MOG_{35–55}$ ($NLP_{ITE+MOG}$) to target AhR for the therapeutic induction of antigen-specific tolerance (Fig. 3*A*). Empty NLPs (NLP) or NLPs loaded only with ITE or $MOG_{35–55}$ were used as controls (NLP_{ITE} or NLP_{MOG}, respectively).

NLPs were, on average, 100 nm in size (ranging from 102.1 ± 28.2 to 104.8 ± 28.1), with a low polydispersity index (<0.06) and a negative charge (zeta potential ranging from −23 to −27 mV) (Fig. 3*B*). ITE is a hydrophobic molecule encapsulated within the lipid bilayer, and $MOG_{35–55}$ is a water-soluble peptide encapsulated within the hydrophilic liposome core; coencapsulation did not alter the encapsulation efficiency of either ITE or $MOG_{35–55}$ (Fig. 3*B*). Indeed, both $NLP_{ITE+MOG}$ and NLP_{ITE} induced the expression of AhR transcriptional targets *Cyp1a1* and *Cyp1b1* to levels similar to those induced by free ITE (Fig. 3*C*), suggesting that ITE coencapsulation with antigen does not alter its ability to activate AhR.

We (16, 21, 22) and others (20, 42, 43) have shown that AhR activation induces a tolerogenic phenotype in DCs. To study the effects of NLP-based delivery of ITE and antigen on T cell stimulation, we used 2D2 mice which express a transgenic T cell receptor reactive with $MOG_{35–55}$ (44). We detected the proliferation of 2D2 splenocytes in response to treatment with either NLP_{MOG} or free $MOG_{35–55}$ (Fig. 3*D*), indicating that NLP-encapsulated $MOG_{35–55}$ is presented to and activates T cells. However, the incorporation of ITE into $MOG_{35–55}$-containing NLPs ($NLP_{ITE+MOG}$) resulted in reduced T cell proliferation (Fig. 3*D*). Taken together with previous reports of the effects of ITE-induced AhR activation on DC APC function, these data suggest that NLP-encapsulated ITE modulates T cell activation by DCs.

NLP Biodistribution. To investigate NLP uptake and biodistribution in vivo, we encapsulated the fluorescent dye 1,1′-dioctadecyl-3,3,3′,3′-tetramethylindo carbocyanine perchlorate (DiI) which is

Downloaded at Palestinian Territory, occupied on November 30, 2021
www.manaraa.com

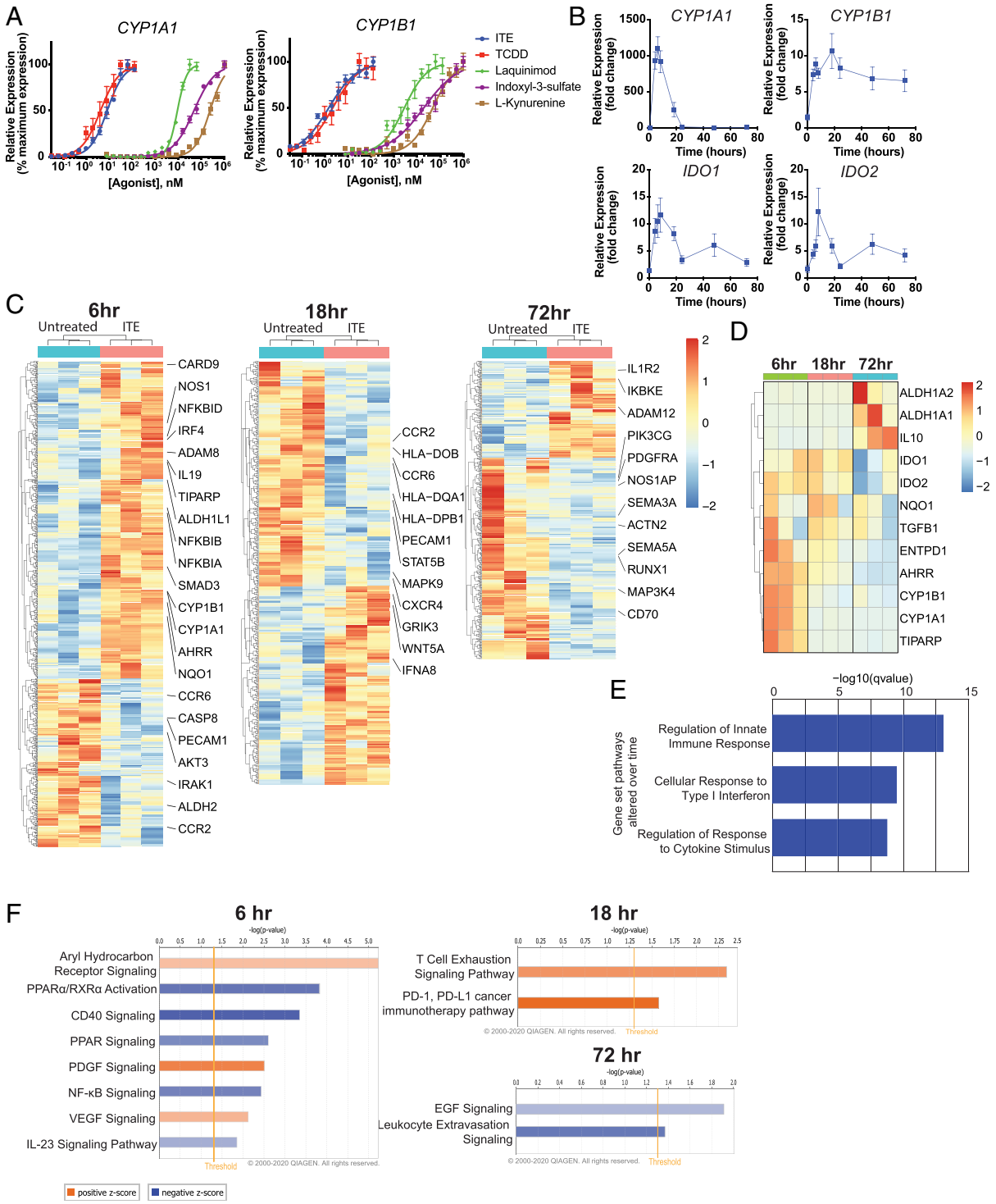

Fig. 1. Temporal regulation of gene expression by AhR ligands in human DCs. (*A*) mRNA expression of the AhR target genes *CYP1A1* and *CYP1B1* in human peripheral blood DCs following incubation for 6 h with ITE, TCDD, laquinimod, indoxyl-3-sulfate, or L-kynurenine. Data were normalized to *GAPDH*, made relative to untreated samples, and presented here as a percentage of maximal induction. Data show the average of two independent experiments with DCs isolated from one independent healthy human donor per experiment. (*B*) mRNA expression of AhR target genes *CYP1A1*, *CYP1B1*, *IDO1*, and *IDO2* in human peripheral blood DCs following incubation with 100 nM ITE for 0, 4, 6, 8, 18, 24, 48, and 72 h. Data are normalized to *GAPDH* and relative to time 0. Data show the average of three independent experiments with DCs isolated from one independent healthy human donor per experiment. (*C*) Heat map of differentially regulated genes determined by SMART-seq RNA-seq in DCs isolated from peripheral blood of three independent healthy human donors and treated for 6, 18, or 72 h with 100 nM ITE. Gene expression is row centered, log2 transformed, and saturated at −2 and +2 for visualization. (*D*) Heat map of expression of 12 genes known to be regulated by AhR activity as determined by SMART-seq RNA-seq in human peripheral DCs treated with 100 nM ITE for 6, 18, or 72 h. Gene expression is row centered, log2 transformed, and saturated at −2 and +2 for visualization. (*E*) Pathways identified by gene set enrichment analysis which were significantly altered over time following treatment in human peripheral blood DCs treated with ITE. (*F*) Ingenuity pathway analysis of the transcriptional profile of human peripheral blood DCs treated with ITE for 6, 18, or 72 h. Pathways associated with positive z-score are in orange; pathways associated with negative z-score are in blue; the relative strength of the z-score is represented by the intensity of the color.

Downloaded at Palestinian Territory, occupied on November 30, 2021

www.manaraa.com

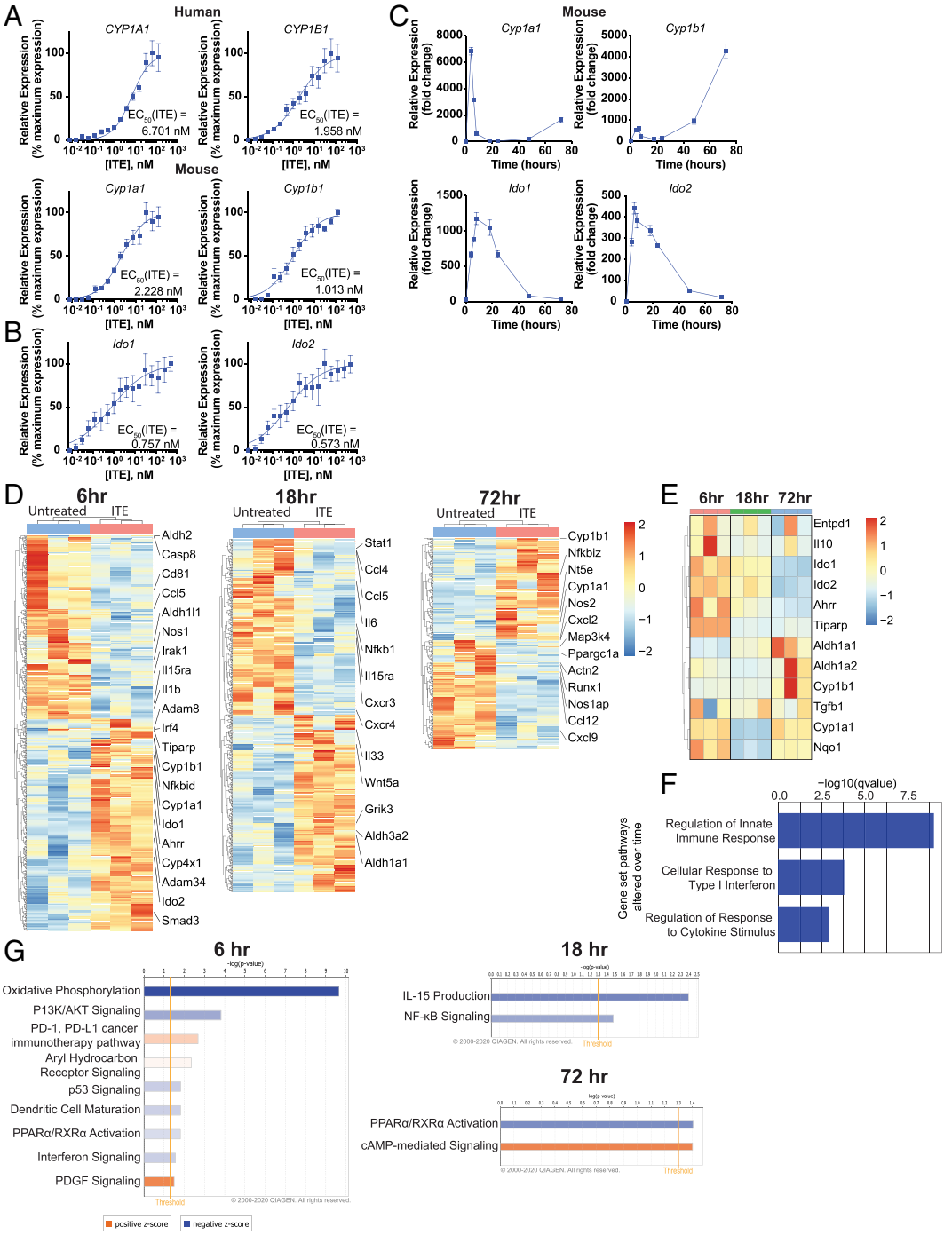

Fig. 2. Temporal regulation of gene expression by AhR ligands in murine DCs. (*A*) mRNA expression of AhR target genes *Cyp1a1* and *Cyp1b1* in human peripheral blood DCs or murine splenic DCs following incubation for 6 h with ITE. Data were normalized to *Gapdh*, made relative to untreated samples, and presented here as a percentage of maximal induction. Data show the average of three independent experiments with DCs isolated from one independent healthy human donor per experiment or a pool of DCs isolated from the spleens of 10 healthy B6 mice. (*B*) mRNA expression of AhR target genes *Ido1* and *Ido2* in murine splenic DCs following incubation for 6 h with ITE. Data were normalized to *Gapdh*, made relative to untreated samples, and presented here as a percentage of maximal induction. Data show the average of two independent experiments with DCs isolated from spleens of 10 healthy B6 mice per experiment. (*C*) mRNA expression of AhR target genes *Cyp1a1*, *Cyp1b1*, *Ido1*, and *Ido2* in murine splenic DCs following incubation with 100 nM ITE for 0, 4, 6, 8, 18, 24, 48, and 72 h. Data are normalized to *Gapdh* and relative to time 0. Data are means ± SEM of one experiment representative of two independent experiments. (*D*) Heat map of differentially regulated genes determined by 3′ DGE-seq RNA-seq in murine splenic DCs isolated from three different pools of 10 mice each and treated for 6, 18, or 72 h with 100 nM ITE. Gene expression is row centered, log2 transformed, and saturated at −2 and +2 for visualization. (*E*) Heat map of the expression of 12 genes known to be regulated by AhR activity as determined by 3′ DGE-seq RNA-seq in murine splenic DCs treated with 100 nM ITE for 6, 18, or 72 h. Gene expression is row centered, log2 transformed, and saturated at −2 and +2 for visualization. (*F*) Pathways identified by gene set enrichment analysis which were significantly altered over time following treatment in murine splenic DCs treated with ITE. (*G*) Ingenuity pathway analysis of the transcriptional profile of murine splenic DCs treated with ITE for 6, 18, or 72 h. Pathways associated with positive z-score are in orange; pathways associated with negative z-score are in blue; the relative strength of the z-score is represented by the intensity of the color.

Downloaded at Palestinian Territory, occupied on November 30, 2021
www.manaraa.com

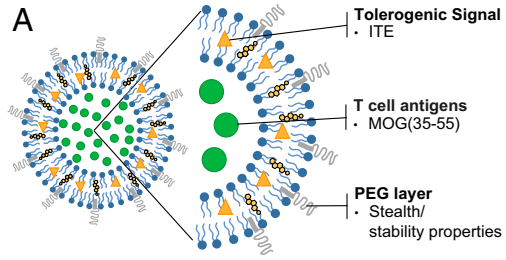

B

	Size (nm)	Polydispersity Index (PDI)	Zeta potential	% Encap. (ITE)	% Encap. (peptide)
NLP	102.4± 27.0	0.042± 0.012	-26.1± 9.8	N/A	N/A
NLP_{ITE}	104.8± 28.1	0.047± 0.010	-26.8± 9.8	63.9± 2.8	N/A
NLP_{MOG}	102.1± 28.2	0.051± 0.014	-23.9± 9.5	N/A	54.3± 6.8
$NLP_{ITE+MOG}$	103.4± 28.3	0.048± 0.011	-24.9± 9.7	61.0± 2.3	54.8± 11.2

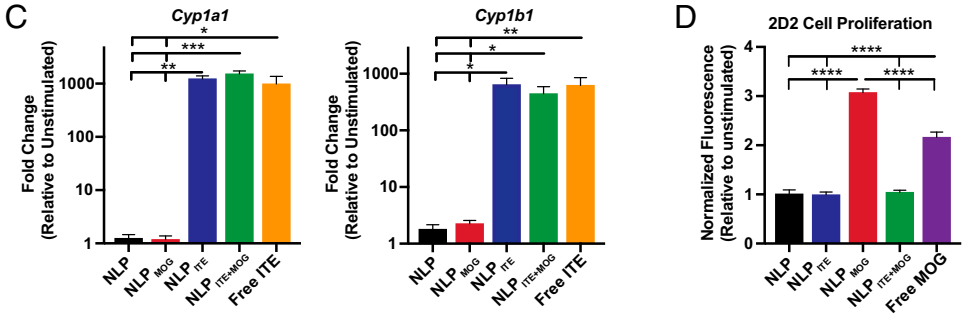

Fig. 3. NLPs loaded with $MOG_{35–55}$ and the tolerogenic AhR ligand ITE. (*A*) Schematic representation of $NLP_{ITE+MOG}$. (*B*) NLP characterization, including size, polydispersity index (PDI), zeta potential, % ITE, and % $MOG_{35–55}$ encapsulation. Values represent the average of at least 17 different batches ± SD. (*C*) mRNA expression of AhR target genes *cyp1a1* and *cyp1b1* in murine splenic DCs following incubation for 6 h with NLP, NLP_{MOG}, NLP_{ITE} (containing 10 nM ITE), $NLP_{ITE+MOG}$ (containing 10 nM ITE), or free ITE (10 nM). (*D*) Proliferative response of 2D2 transgenic splenocytes activated for 72 h with NLP, NLP_{MOG} (containing 10 μg/mL MOG), NLP_{ITE} (containing 1 μg/mL ITE), $NLP_{ITE+MOG}$ (containing 10 μg/mL MOG and 1 μg/mL ITE), or free MOG (10 μg/mL). Data from *C* and *D* are means + SEM of one experiment representative of at least three independent experiments, with at least three biological replicates per experiment. $*P < 0.05$, $**P < 0.01$, $***P < 0.001$, $****P < 0.0001$, one-way ANOVA followed by Dunnett's multiple comparison test.

incorporated into the lipid bilayer (45). Following incubation of splenocytes from naive mice with DiI-labeled NLPs (NLP_{DiI}) for 4 h at 37 °C, we determined by flow cytometry that the majority of NLP_{DiI} were taken up by DCs ($CD11c^+$ cells) and macrophages ($CD11b^+$ cells) (Fig. 4*A*). Indeed, up to 30% of DCs were DiI^+ (Fig. 4*A*). To analyze the uptake of NLPs in vivo, NLP_{DiI} were administered intravenously (IV) or subcutaneously (SC), and spleen and inguinal lymph nodes (LNs) were analyzed 2 h and 18 h later. NLP_{DiI} were taken up mostly by DCs, macrophages, and B cells (Fig. 4*B*); DCs showed the highest uptake of NLP_{DiI}.

NLP-Delivered ITE Induces a Tolerogenic Phenotype in Mouse and Human DCs. AhR activation in DCs has been linked to the induction of a tolerogenic phenotype (16, 20–22, 42, 43). Thus, we cultured splenic DCs from naive C57BL6/J (B6) mice for 6 h with NLP, NLP_{ITE}, NLP_{MOG}, or $NLP_{ITE+MOG}$ to study their effects on pro- and antiinflammatory gene expression (Fig. 4*C*). Treatment with $NLP_{ITE+MOG}$ or NLP_{ITE} increased the expression of antiinflammatory genes such as *Il10*, *Tgfb*, *Ido1*, and *Ido2*. $NLP_{ITE+MOG}$ and NLP_{ITE} also limited the expression of proinflammatory cytokines (e.g., *TNFα* and *IL6*) induced by lipopolysaccharide (LPS).

We also studied the effects of NLPs on human DCs isolated from the peripheral blood mononuclear cells (PBMCs) of three healthy human donors, cultured in vitro with NLP or NLP_{ITE} for 6 h (Fig. 4*D*). NLP_{ITE} up-regulated the expression of AhR target genes *CYP1A1* and *CYP1B1*, and also of the antiinflammatory genes *IL10* and *TGFB*. Moreover, NLP_{ITE} limited the expression of *IL6* and *IL12* induced by LPS. Taken together, these data suggest that NLP-delivered ITE induces a tolerogenic phenotype in DCs.

NLPs Ameliorate Acute Experimental Autoimmune Encephalomyelitis in C57BL/6J Mice. To evaluate the therapeutic potential of tolerogenic NLPs in experimental autoimmune encephalomyelitis (EAE), we administered $NLP_{ITE+MOG}$ to C57BL/6J mice, (SC) once a week beginning the day after $MOG_{35–55}$ immunization, or only once on day 7 after EAE induction (IV). Empty NLPs, NLP_{ITE}, or NLP_{MOG} were used as controls. $NLP_{ITE+MOG}$ administration, either SC (Fig. 5*A*) or IV (Fig. 5*B*), suppressed EAE development. Moreover, a single $NLP_{ITE+MOG}$ IV administration 15 d after disease induction suppressed ongoing EAE (Fig. 5*C*).

To evaluate the durability of the protection induced by NLPs, empty NLPs or $NLP_{ITE+MOG}$ were administered IV on 3 consecutive days, 1 mo, 2 wk, 1 wk, or 1 d prior to EAE induction. $NLP_{ITE+MOG}$ administration reduced EAE development even when administered 1 mo prior to disease induction, indicating that the tolerance induced by $NLP_{ITE+MOG}$ is long lasting (Fig. 5*D*).

To characterize the immunological effects of $NLP_{ITE+MOG}$, we studied the T cell recall response 26 d after EAE induction following SC NLP administration as shown in Fig. 5*A*. $NLP_{ITE+MOG}$ administration suppressed the proliferative recall response to $MOG_{35–55}$; reduced the production of proinflammatory cytokines, including IL-17, IFNγ, and TNFα; and increased antiinflammatory IL-10 detected in culture supernatants (Fig. 6 *A* and *B*).

EAE is driven by $MOG_{35–55}$-specific T_H1 and T_H17 cells. Therefore, we used a $MOG_{38–49}$/$I\text{-}A^b$ tetramer in combination with intracellular cytokine staining to quantify $MOG_{35–55}$-reactive T_H1 and T_H17 cells (46) (Fig. 6*C*). We detected a reduction in $MOG_{35–55}$-specific $IL\text{-}17^+$ and $IFN\gamma^+$ $CD4^+$ cells in the central nervous system (CNS) of $NLP_{ITE+MOG}$-treated mice (Fig. 6*D*). In addition, $NLP_{ITE+MOG}$ treatment increased $MOG_{35–55}$-specific $FoxP3^+$ and $IL\text{-}10^+$ $CD4^+$ T cells in the CNS (Fig. 6 *C* and *D*), and consequently, the regulatory/effector T cell balance in the CNS. Taken together, these findings suggest that NLPs modulate disease-promoting T cells in an antigen-specific manner.

NLPs Induce Bystander Tolerance. The pathology of most human autoimmune diseases involves intra- and intermolecular epitope spreading (47, 48), resulting in the targeting of multiple epitopes by the pathogenic autoimmune response. Thus, the induction of bystander tolerance is considered an important feature to maximize the chances of success of tolerogenic immunotherapies for

Downloaded at Palestinian Territory, occupied on November 30, 2021
www.manaraa.com

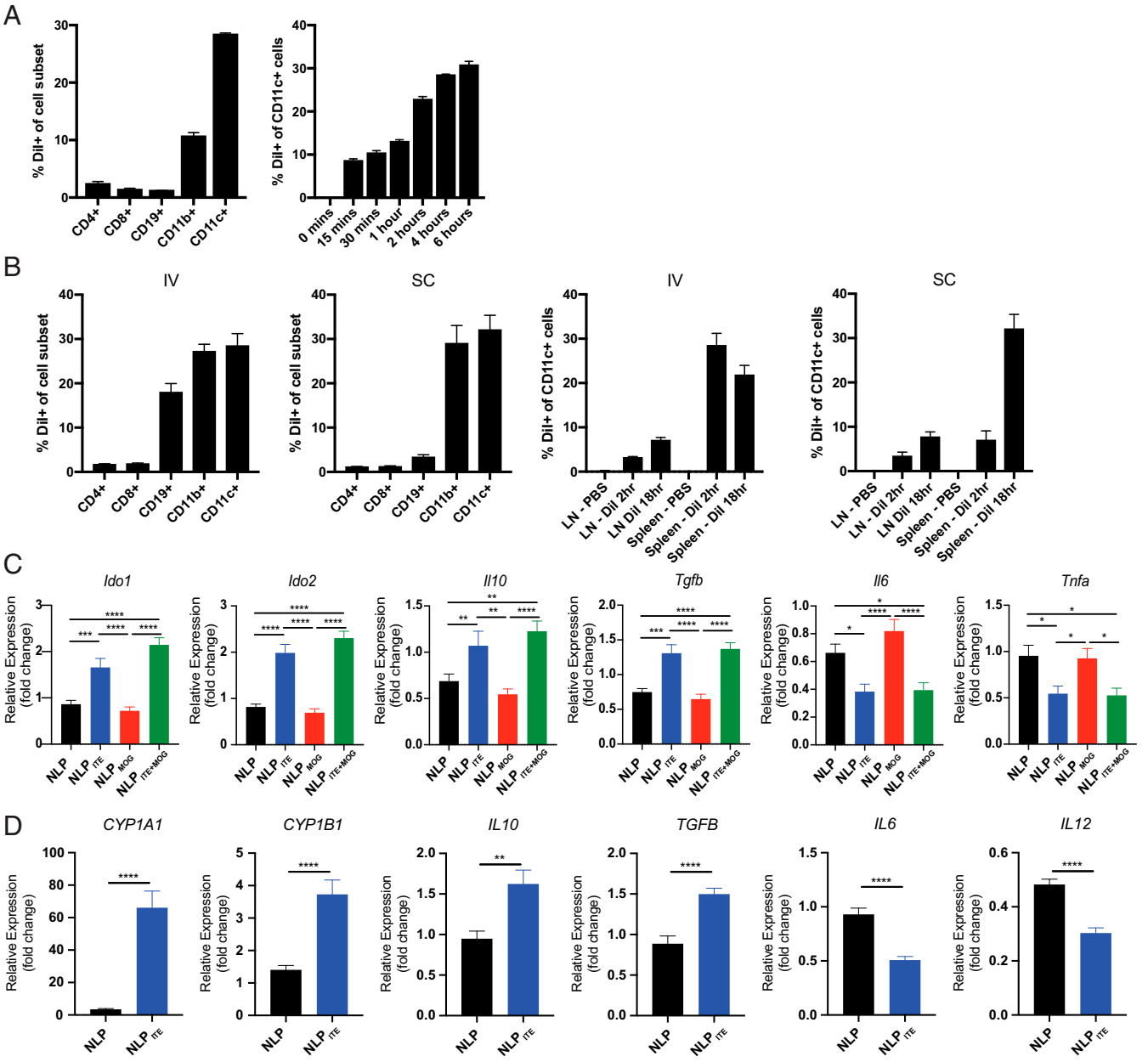

Fig. 4. $NLP_{ITE+MOG}$ induces a tolerogenic phenotype in mouse and human DCs. (*A*) Murine splenocytes were isolated and cultured for 4 h in vitro with NLP_{DiI} and examined by flow cytometry for NLP_{DiI} uptake (*Left*). NLP_{DiI} uptake by $CD11c^+$ cells was measured at various timepoints (15 min to 6 h) (*Right*). (*B*) NLP_{DiI} uptake by splenocytes as evaluated by flow cytometry 2 h after IV or SC NLP injection (*Left* two). NLP_{DiI} uptake in spleen or LN $CD11c^+$ cells measured 2 h or 18 h after IV or SC NLP injection (*Right* two). (*C*) *Ido1*, *Ido2*, *Il10*, *TGFβ*, *Il6*, and *Tnfα* expression in murine splenic DCs after culture for 6 h in vitro with NLP, NLP_{MOG}, NLP_{ITE}, or $NLP_{ITE+MOG}$. For evaluation of *Il6* and *Tnfα*, murine splenic DCs were stimulated with LPS during culture with NLPs. Data are depicted as the mean + SEM of three independent experiments with three biological replicates per experiment. (*D*) Human DCs were isolated from three independent healthy donor PBMCs, cultured for 6 h in vitro with NLP or NLP_{ITE} and *CYP1A1*, *CYP1B1*, *IL10*, *TGFβ*, *IL6*, and *IL12* expression was analyzed by RT-PCR. For evaluation of *IL6* and *IL12*, DCs were stimulated with LPS during culture with NLPs. Data are depicted as the mean + SEM of three independent healthy donors. $*P < 0.05$, $**P < 0.01$, $***P < 0.001$, $****P < 0.0001$, one-way ANOVA followed by Dunnett's multiple comparison test, or Student's *t* test.

human autoimmune disorders. To determine whether ITE-loaded NLPs promote bystander suppression, we induced EAE in C57BL/6 × SJL F1 mice by immunization with proteolipid protein $(PLP)_{139–151}$ peptide in complete Freund's adjuvant (CFA) and treated the mice SC with NLPs loaded with ITE and $PLP_{139–151}$ (the myelin epitope used to induce EAE; $NLP_{ITE+PLP}$), $MOG_{35–55}$ (a myelin epitope noncross-reactive with $PLP_{139–151}$; $NLP_{ITE+MOG}$), or an irrelevant peptide ($NLP_{ITE+IrrPep}$). Treatment with either $NLP_{ITE+PLP}$ or $NLP_{ITE+MOG}$, but not $NLP_{ITE+IrrPep}$, ameliorated EAE (Fig. 7*A*). Moreover, $NLP_{ITE+PLP}$ or $NLP_{ITE+MOG}$ administration led to a reduced proliferative recall response to $PLP_{139–151}$, reduced production of proinflammatory cytokines, including IL-17 and IFNγ, and a concomitant increase in IL-10 (Fig. 7 *B* and *C*). $NLP_{ITE+PLP}$ or $NLP_{ITE+MOG}$ administration also suppressed the infiltration of pathogenic effector T cells into the CNS, as evidenced by a reduction in the relative expression of *Il17*, *Ifnγ*, and *Il1b* mRNA (Fig. 7*D*), while increasing the percentage of regulatory $IL\text{-}10^+$ CD4 T cells in the CNS (Fig. 7*E*). Collectively, these findings suggest that the codelivery of ITE and tissue-specific antigens with NLPs induces bystander tolerance,

Downloaded at Palestinian Territory, occupied on November 30, 2021
www.manaraa.com

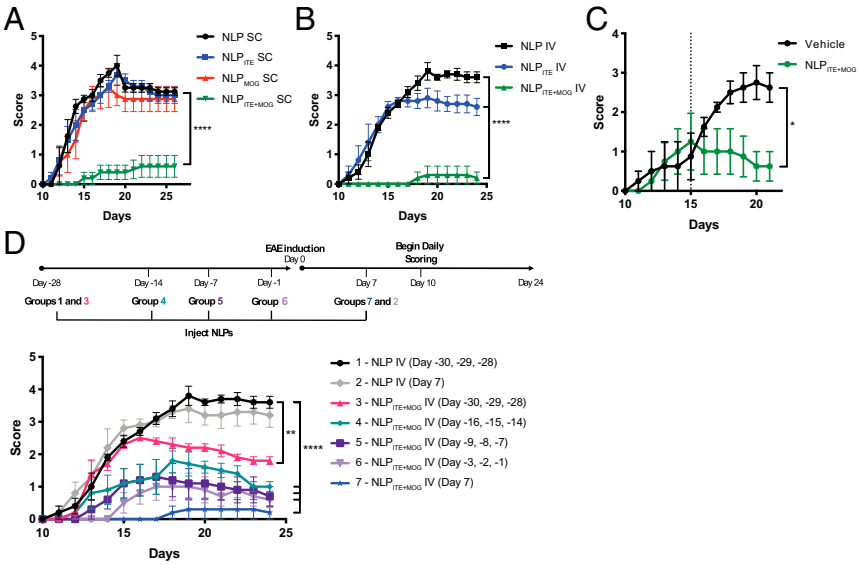

Fig. 5. NLP$_{ITE+MOG}$ suppresses acute EAE in C57BL/6J mice. EAE was induced in B6 mice with MOG$_{35–55}$, and NLPs were administered following various treatment regimens. (*A*) Clinical scores of mice treated SC with NLPs once a week beginning the day after disease induction. (*B*) Clinical scores of mice treated IV with NLPs administered once on day 7 after disease. (*C*) Clinical scores of mice treated IV with NLPs administered once on day 15 after disease. (*D*) Clinical scores of mice treated daily IV with NLPs for 3 d 1 mo prior, 2 wk prior, 1 wk prior, 1 d prior, or a single injection 1 wk after EAE induction. Data are mean ± SEM ($n = 5$ mice per group). $*P < 0.05$, $**P < 0.01$, $****P < 0.0001$, two-way repeated measures ANOVA followed by Tukey's multiple comparison test.

limiting the pathogenic autoimmune response directed against other autoantigens expressed in the same tissue.

NLPs Ameliorate Chronic Progressive NOD EAE. NOD mice immunized with MOG$_{35–55}$ develop a chronic progressive form of EAE, which starts ∼25 d after immunization and resembles some aspects of secondary progressive MS (SPMS), including the chronic activation of astrocytes and microglia thought to drive the progressive accumulation of neurodegeneration and axonal loss (49, 50). To further evaluate the therapeutic potential of NLP$_{ITE+MOG}$, we initiated weekly SC administration of NLP$_{ITE+MOG}$ 35 d after EAE induction, during the chronic phase of NOD EAE; NLP, NLP$_{ITE}$, and NLP$_{MOG}$ were used as controls. Treatment with NLP$_{ITE+MOG}$ suppressed EAE symptoms as measured by clinical scores (Fig. 8*A*). In addition, we detected fewer CNS-infiltrating CD11b^{+}CD45^{+}Ly6C^{hi} proinflammatory monocytes in NLP$_{ITE+MOG}$-treated mice (Fig. 8*B*).

IL-10 produced by Tr1 cells has been shown to limit proinflammatory responses in astrocytes and microglia (51). We detected increased MOG-specific IL-10^{+} CD4^{+} T cells in the CNS of NOD EAE mice treated with NLP$_{ITE+MOG}$ (Fig. 8*C*). Moreover, the analysis of astrocytes, microglia, and CNS-recruited monocytes by RNA-seq detected the down-regulation of proinflammatory transcriptional modules in NLP$_{ITE+MOG}$-treated NOD EAE mice (Fig. 8 *D*–*G*), including those associated with NF-κB activation and the production of chemokines and cytokines. This down-regulation of the proinflammatory response of astrocytes, microglia, and monocytes induced by NLP$_{ITE+MOG}$ treatment was concomitant with the up-regulation of IL-10Rα signaling (z-score 6.810, *P* value 3.27E^{-37}, Fig. 8*H*). In summary, NLP$_{ITE+MOG}$ decreased the expression of proinflammatory transcriptional programs thought to contribute to the pathogenic role of astrocytes, microglia, and monocytes in MS and NOD EAE.

Discussion

There is an unmet medical need for therapeutic approaches to induce antigen-specific immune tolerance. These approaches offer numerous advantages over current immunosuppressive therapies, often associated with debilitating and/or life-threatening side effects. Multiple strategies for antigen-specific tolerance induction have been explored, including the administration of whole protein autoantigens, altered or unaltered peptide ligands, DNA vaccines, and the delivery of peptides complexed to major histocompatability complex (MHC) or loaded onto nanoparticles (52–59). However, recent advances in nanotechnology offer exciting opportunities for antigen-specific immunotherapy, overcoming limitations linked to other tolerance-inducing strategies.

Nanomaterials such as metal-based particles, polymeric particles, and lipid-based particles have shown success as carriers of tolerogenic agents and antigens (21, 22, 58, 60–62). Indeed, nanoparticles have been used to target specific cell types, codeliver multiple therapeutic agents to the same cell, facilitate the transport of drugs across biological barriers, and protect encapsulated therapeutic agents from in vivo degradation and clearance (21, 22, 58, 60, 61). In this work, we describe the use of NLPs to codeliver the tolerogenic AhR ligand ITE and disease-specific peptide antigens, to induce antigen-specific tolerance and suppress disease in three preclinical mouse models of MS. The amelioration of EAE was associated with a reduction in myelin-specific T$_H$1 and T$_H$17 effector cells, an increase in antigen-specific Treg cells, and the suppression of disease-promoting inflammatory modules in CNS resident astrocytes and microglia. These findings are in agreement with our previous studies using gold nanoparticles loaded with ITE and antigen to induce tolerance in experimental models of MS and type 1 diabetes (21, 22). However, NLPs offer several advantages when compared to other nanomaterial approaches, because they employ manufacturing methods which are easily scalable, based on FDA-approved materials, and have already been tested in the clinic (26, 27). In addition, NLPs provide fine control of small molecule and antigen loading. Finally, NLPs are well characterized as drug delivery vehicles and considered safe for human use based on the available clinical experience with FDA-approved liposome-based drug products (26, 27).

Importantly, the NLP-based approach described here induced bystander suppression in the C57BL/6 × SJL F1 mouse model of EAE. This bystander suppression likely results from the induction of tolerogenic DCs by both cell-intrinsic effects driven by AHR signaling, as suggested by our transcriptional analyses, and also by DC interactions with antigen-specific regulatory T cells (63). In addition, regulatory T cells recruited to inflamed sites can also control local inflammation via the secretion of soluble factors and additional mechanisms (37, 51, 64). Since most autoimmune diseases, including MS, are characterized by intra- and intermolecular epitope spreading (47, 48), the induction of bystander suppression is considered critical for the success of antigen-specific therapeutics. Indeed, although high-throughput methods enabled the identification of disease-associated

Downloaded at Palestinian Territory, occupied on November 30, 2021

www.manaraa.com

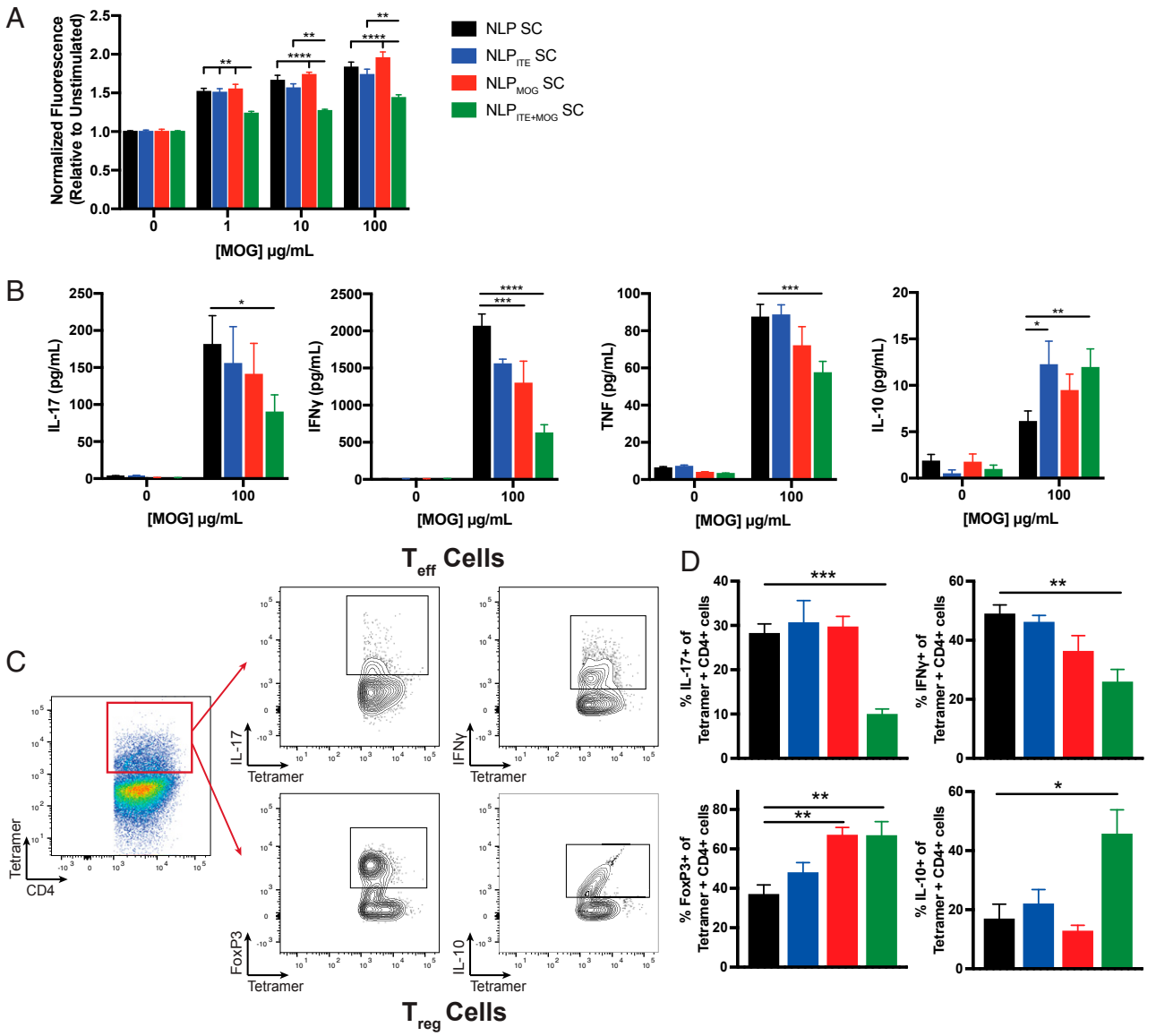

Fig. 6. $NLP_{ITE+MOG}$ suppresses the encephalitogenic T cell response. (*A*) Proliferative response and (*B*) cytokine secretion following restimulation with $MOG_{35–55}$ of splenocytes from SC NLP-treated B6 mice, 26 d after EAE induction. (*C*) Gating strategy for the identification of $MOG_{38–49}$ tetramer-positive IL-17$^+$, IFNγ$^+$, FoxP3$^+$, and IL-10$^+$ CD4$^+$ T cells. (*D*) Frequency of $MOG_{38–49}$ tetramer-positive IL-17$^+$, IFNγ$^+$, FoxP3$^+$, and IL-10$^+$ CD4$^+$ T cells in the brain and spinal cord of B6 EAE SC NLP-treated mice. Data are mean + SEM ($n = 5$ mice per group). *$P < 0.05$, **$P < 0.01$, ***$P < 0.001$, ****$P < 0.0001$, one-way ANOVA followed by Dunnett's multiple comparison test.

autoantigens and the monitoring of epitope spreading (53, 65–70), our knowledge is still incomplete regarding the totality of the autoantigens targeted in different autoimmune diseases and the heterogeneity of these autoimmune responses among different patients afflicted by the same disease or in different disease phases. Hence, the induction of functional bystander suppression provides further support for the use of the NLP-based tolerogenic approaches described here for the treatment of human autoimmunity.

Despite their efficacy in preclinical models, certain challenges must be considered when using nanomaterial-based approaches for the therapeutic reestablishment of immune tolerance in human inflammatory disorders. In particular, manufacturing and scale up can be challenging given the complex nature of these therapeutics. However, these challenges have already been overcome during the production of other NLP-based therapeutics (26, 71). Hence, NLPs engineered to codeliver tolerogenic small molecules and disease-associated antigens may provide an efficacious approach for the therapeutic reestablishment of antigen-specific tolerance in human autoimmunity.

Materials and Methods

Mice and Reagents. Female C57BL/6J and NOD/ShiLtJ mice were obtained from The Jackson Laboratory and maintained in a pathogen-free facility at the Charles River Accelerator and Development Labs (CRADL). All experiments were carried out in accordance with guidelines prescribed by the Institutional Animal Care and Use Committee at CRADL. ITE was purchased from Tocris Biosciences. TCDD, laquinimod, indoxyl-3-sulfate, and L-kynurenine were purchased from Sigma-Aldrich.

Liposome Preparation. Liposomes were prepared by the ethanol injection method (38). Briefly, ITE (Tocris Biosciences) (0.5% wt/wt to total lipids) was dissolved in a mixture of egg phosphotidylcholine (EPC, Lipoid GmbH), cholesterol (Corden Pharma), and 1,2 dioleoyl-sn-glycero-3-phosphoethanolamine-*N*-[methoxy(polyethylene glycol)-2000] (mPEG2000-PE, Corden Pharma) in absolute ethanol and stirred until dissolved completely. $MOG_{35–55}$ (GenScript), $PLP_{139–151}$

Downloaded at Palestinian Territory, occupied on November 30, 2021
www.manaraa.com

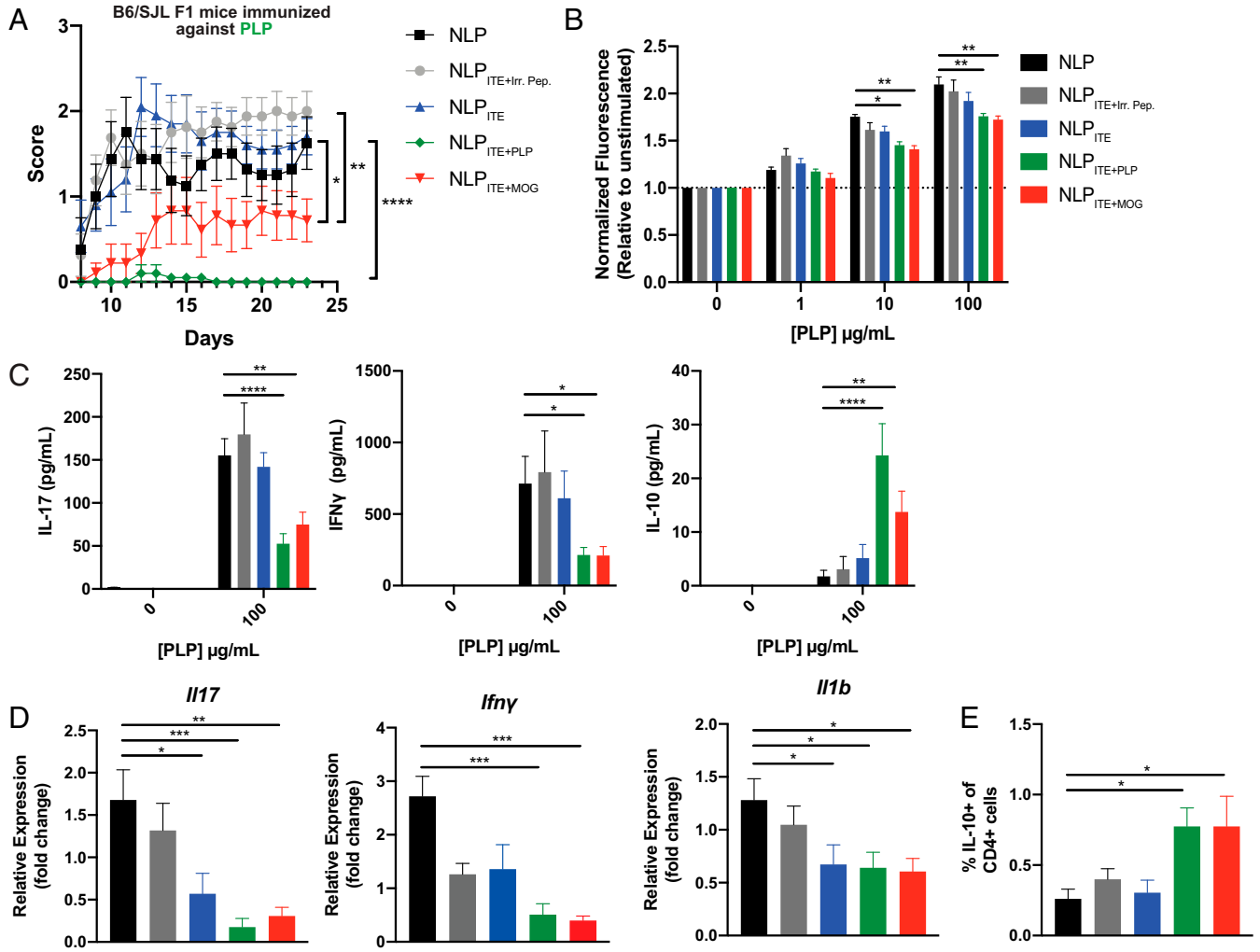

Fig. 7. $NLP_{ITE+MOG}$ ameliorates EAE in B6 × SJL F1 mice induced using PLP. SC NLPs were administered once a week beginning 1 d after disease induction using $PLP_{139–151}$ in C57BL/6 × SJL F1 mice. (*A*) Clinical scores of NLP-treated mice (graph shows the average ±SEM of two independent experiments with $n = 5$ mice per group, per experiment. $^*P < 0.05$, $^{**}P < 0.01$, $^{***}P < 0.001$, $^{****}P < 0.0001$, two-way repeated measures ANOVA followed by Tukey's multiple comparison test). (*B*) Proliferative response and (*C*) cytokine secretion following restimulation with $PLP_{139–151}$ of splenocytes from NLP-treated mice, 24 d after EAE induction. Data are mean + SEM with $n = 4$ mice per group, representative of two independent experiments. $^*P < 0.05$, $^{**}P < 0.01$, $^{***}P < 0.001$, $^{****}P < 0.0001$ (*B*), two-way ANOVA followed by Dunnett's multiple comparison test. (*C*) One-way ANOVA followed by Dunnett's multiple comparison test. (*D*) Relative mRNA expression of *Il17*, *Ifnγ*, and *Il1b* in the CNS of NLP-treated mice. (*E*) Frequency of IL-10^+ $CD4^+$ T cells in the CNS of NLP-treated mice. (*D* and *E*) Data are mean + SEM ($n = 8$ mice per group, average of two independent experiments). $^*P < 0.05$, $^{**}P < 0.01$, $^{***}P < 0.001$, $^{****}P < 0.0001$, one-way ANOVA followed by Dunnett's multiple comparison test.

(GenScript), or irrelevant peptide (in this case, ω-$Gliadin_{102–118}$ [GenScript]) was added to Hepes buffered saline (HBS), pH 6.5, at the desired concentration, and stirred. The lipid-ITE mixture was then added to the peptide solution under constant stirring to obtain multilamellar vesicles (MLVs). The liposomes were stirred for 1.5 h after which they were sequentially extruded five times through Nucleopore polycarbonate membranes (400-, 200-, and 100-nm pore size) using a 10-mL LIPEX extruder (Evonik). The liposomes were purified through G-25 sephadex resin using PD-10 columns (GE Healthcare) and finally filtered through 0.22-µm polyethersulfone filters to sterilize them. For some studies, the liposomes were fluorescently labeled by encapsulating DiIC18(5)-DS (1,1′-dioctadecyl-3,3,3′,3′-tetramethylindodicarbocyanine-5,5′-disulfonic acid) dye, added at 0.35 mol% relative to egg phophatidylcholine. The phospholipid concentration was determined by using a modified Bartlett method. The final drug/phospholipid molar ratio was ∼0.015. Liposomes were characterized for size, polydispersity, zeta potential, ITE, and antigen loading. ITE concentration was determined spectrophotometrically at 355 ± 2 nm after lysing the liposomes using methanol containing 1% acetic acid. Antigen concentration was determined using the fluorescence-based CBQCA (3-(4-carboxybenzoyl)quinoline-2-carboxaldehyde) assay after lysing liposomes with sodium borate (0.1 M) containing 0.5% Triton-X 100. The % drug/antigen loading was determined by dividing the drug/antigen amount determined in the final formulation by the initial amount used during liposome preparation.

Purification of DCs. Splenic mouse DCs were purified from naive B6 mice using the pan DC isolation kit according to the manufacturer's instructions (Miltenyi). Human DCs were purified from healthy donor leukopaks purchased from Research Blood Components using the Blood Dendritic Cell Isolation Kit II following the manufacturer's instructions (Miltenyi).

EAE Induction and Treatment. EAE was induced in 8- to 10-wk-old female mice by SC immunization with 200 µg $MOG_{35–55}$ peptide or $PLP_{139–151}$ emulsified in CFA (Hooke Laboratories) per mouse, followed by administration of 400 ng pertussis toxin (Hooke Laboratories) on days 0 and 2 as described (49). Clinical signs of EAE were assessed as follows: 0, no signs of disease; 1, loss of tone in the tail; 2, hind limb paresis; 3, hind limb paralysis; 4, tetraplegia; 5, moribund. For B6 or B6 × SJL F1 EAE, mice were treated with NLPs either SC once a week beginning on day 1 after disease induction, IV once on day 7 for disease prevention, or once on day 15 for disease reversal, as outlined in the specific experiments. For NOD EAE, mice were treated SC with NLPs or HBS once a week beginning on day 35 after disease induction.

Downloaded at Palestinian Territory, occupied on November 30, 2021

www.manaraa.com

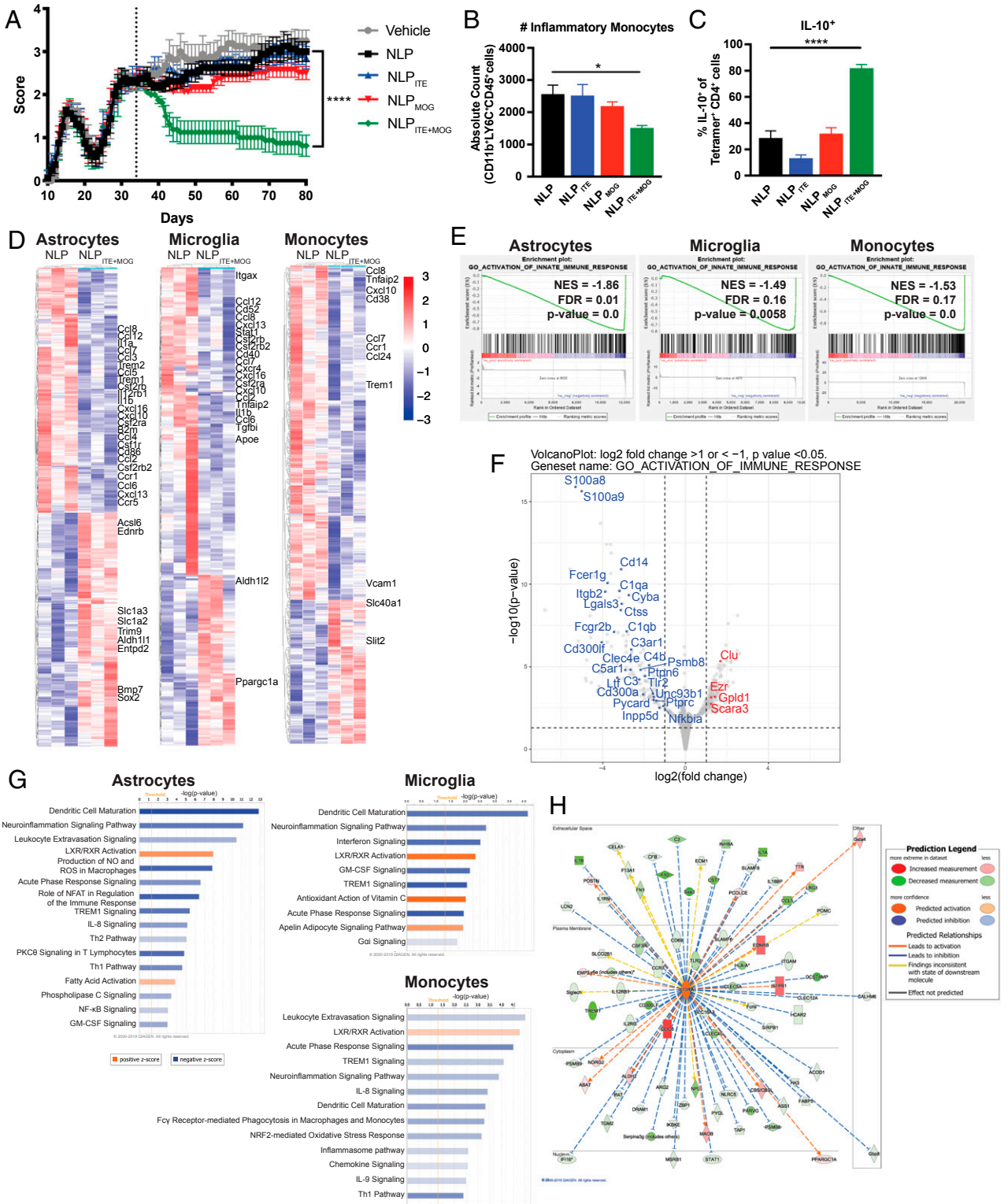

Fig. 8. $NLP_{ITE+MOG}$ ameliorates chronic progressive NOD EAE. SC NLPs were administered once a week beginning on day 35 after NOD induction. (*A*) Clinical scores of NLP-treated mice ($n = 10$ mice per group, representative of two independent experiments. $^{****}P < 0.0001$, two-way repeated measures ANOVA followed by Tukey's multiple comparison test). (*B*) CNS-infiltrating $CD11b^+CD45^+Ly6C^{hi}$ monocytes determined by flow cytometry ($n = 10$ mice per group. $^{****}P < 0.0001$, one-way ANOVA followed by Dunnett's multiple comparison test). (*C*) $MOG_{38–49}$ tetramer-positive IL-10^+ $CD4^+$ T cells in the CNS of NOD EAE SC NLP-treated mice 100 d after EAE induction. ($n = 10$ mice per group. $^{****}P < 0.0001$, one-way ANOVA followed by Dunnett's multiple comparison test.) (*D*) Heat map of differentially regulated genes determined by SMART-seq RNA-seq in astrocytes, microglia, and monocytes from NLP- or $NLP_{ITE+MOG}$-treated mice on day 100 after NOD EAE induction. Gene expression is row centered, log2 transformed, and saturated at −3 and +3 for visualization. (*E*) Gene set enrichment analysis correlation of genes associated with innate immunity. (*F*) Volcano plot depicting differentially expressed genes associated with activation of the immune response in astrocytes of $NLP_{ITE+MOG}$-treated NOD EAE mice. (*G*) Ingenuity pathway analysis of the transcriptional profile of astrocytes, microglia, and monocytes. (*H*) Ingenuity pathway analysis of the IL10Rα signaling pathway in astrocytes from $NLP_{ITE+MOG}$-treated NOD EAE mice.

Downloaded at Palestinian Territory, occupied on November 30, 2021
www.manaraa.com

Throughout, NLPs were administered at the following doses: NLP_{ITE} containing 7 μg ITE, NLP_{MOG} containing 3 to 5 μg $MOG_{35–55}$, $NLP_{ITE+MOG}$ containing 7 μg ITE and 3 to 5 μg $MOG_{35–55}$, $NLP_{ITE+PLP}$ containing 7 μg ITE and 3 to 5 μg $PLP_{139–151}$, $NLP_{ITE+Irr.\ Pep.}$ containing 7 μg ITE and 3 to 5 μg of a T cell epitope from wheat gliadin, or empty NLPs dosed to match the highest lipid content administered. Scoring of the clinical symptoms in some of the B6 studies, and all of the B6 × SJL F1 EAE and NOD EAE studies was performed by a researcher blinded to the group identification.

T Cell Proliferation. Splenocytes were plated at a density of 4×10^5 cells per well in a 96-well round-bottom plate and cultured in complete medium (RPMI with Glutamax and 10% fetal bovine serum, with penicillin/streptomycin) with increasing concentrations of $MOG_{35–55}$ or $PLP_{139–151}$ peptide for 72 h at 37 °C, 5% CO^2. Supernatants were then collected and stored at −20 °C for later analysis of cytokine production. Cells were washed once with phosphate buffered saline (PBS), resuspended in 50 μL of PBS and 10 μL of Cell Titer Blue (Promega), and cultured for an additional 4 h. Fluorescence intensity was measured at a 530-nm excitation wavelength and a 590-nm emission wavelength.

Cytokine Analysis. Cytokine release following splenocyte stimulation for 72 h with 100 μg/mL $MOG_{35–55}$ or $PLP_{139–151}$ peptide was measured using the BD CBA Mouse Th1/Th2/Th17 Cytokine Kit (BD Bioscience) following the manufacturer's instructions. Fluorescence was measured using a BD fluorescence-activated cell sorting (FACS) Canto II Flow Cytometer and analyzed by FCAP ArrayTM Software (BD Bioscience). Individual cytokine concentrations were indicated by their fluorescent intensities and concentrations were determine using cytokine standards.

Tetramer and Intracellular Flow Cytometry Staining on CNS. CNS mononuclear cell suspensions were prepared as described (49). $CD4^+$ T cells were then isolated using the CD4 (L3T4) positive selection kit (Miltenyi Biotec) following the manufacturer's instructions. $CD4^+$ T cells were then stimulated for 6 h with PMA (phorbol 12-myristate 13-acetate; 50 ng/mL; Sigma), ionomycin (1 μg/mL; Sigma), and brefeldin A (Biolegend) and washed and incubated for 30 min with Dasatanib (5 nM, Sigma-Aldrich), followed by a 1-h incubation with control or $MOG_{38–49}$ tetramer. The tetramers used were obtained from the NIH Tetramer core facility: MOG I-A(b) mouse $MOG_{38–49}$ GWYRSPFSRVVH PE-labeled tetramer, and I-A(b) human $CLIP_{87–101}$ PVSKMRMATPLLMQA (control) PE-labeled tetramer. Tetramer-stained cells were then washed, stained with surface markers, and then fixed and made permeable according to the manufacturer's instructions (Foxp3 Fixation/Permeabilization kit) (eBioscience). Cells were analyzed on a BD FACS Canto II. All antibodies were purchased from Biolegend or eBioscience. All surface markers were stained at 1:250 and all intracellular markers were stained at 1:100 unless otherwise recommended by the manufacturer.

FACS of Astrocytes, Monocytes, and Microglia. Astrocytes, monocytes, and microglia were sorted as described (49, 72) using a BD FACS Aria II. Isolated CNS cells were stained with fluorochrome-conjugated antibody to CD11b (M1/70, 1:50), CD45 (90, 1:50), Ly6C (HK1.4. 1:100), CD105 (N418, 1:100), CD140a (APA5, 1:100), CD11 c (N418, 1:100), F4/80 (BM8, 1:50), O4 (O4, Miltenyi Biotec, 1:10), and CD19 (eBio1D3, 1:100). All antibodies were from Biolegend, eBioscience, or BD Pharmingen unless otherwise mentioned. Microglia were sorted as $CD11b^+$ cells with low CD45 expression and low Ly6C ($CD11b^+CD45^{low}Ly6C^{low}$); inflammatory monocytes were considered as $CD45^{hi}$ $CD11b^+Ly6C^{hi}$ (49). Astrocytes were sorted as $CD11b^{low}CD45^{low}$ $Ly6C^{low}CD105^{low}CD140a^{low}CD11bI^{ow}F4/80^{low}O4l\text{-}CD19^{low}$ after the exclusion of lymphocytes, microglia, oligodendrocytes, and monocytes.

RNA Sequencing (SMART-Seq and 3′ Differential Gene Expression). Sequencing was performed at the Broad Institute. The RNA sequencing data were first trimmed using Trim Galore in order to remove adapters and low-quality bases. The sequencing samples were then aligned to the Ensembl Mouse reference genome GRCm38 using STAR (v 2.7.1a) and Kallisto (0.46.0) (73). The software Picard (2.20.4) was used to remove duplicates. RSEM (v 1.3.1) (74) was used to do the quantifications for samples.

Differential gene expression (DGE) analysis was conducted using DESeq2, and the log2 change shrink is conducted by using the package apeglm (75). Differential genes were considered significant if P value <0.05. The results of the differential expression analysis were used for downstream analysis. Pathway analysis was performed using gene set enrichment analysis (4.0.0) and Ingenuity pathway analysis software (Qiagen) on significant genes. Pathways were considered significant if P value <0.05.

The time-course analysis of the RNA-seq data was done using the EBSeqHMM package (76) which uses an empirical Bayesian approach to categorize the expression pattern of genes during the time course.

RT-PCR. RNA was extracted using the RNAeasy kit (Qiagen), cDNA was prepared, and qPCR was run using Gapdh for normalization. Primers and probes were from Thermo Fisher Scientific: for mouse, Cyp1a1 Mm00487218_m1, Cyp1b1 Mm00487229_m1, Gapdh Mm99999915_g1, Ido1Mm00492590_m1, Ido2 Mm00524210_m1, Il6 Mm00446190_m1, Il10 *Mm01288386_m1*, Tgfb1 Mm01178820_m1, Tnfa Mm00443258_m1, *Il17* Mm00439618_m1, and *IL1b* Mm00434228_m1; and for human, CYP1A1 Hs01054796_g1, CYP1B1 Hs02382916_s1, *GAPDH*, Hs02786624_g1, IL6 Hs00985639_m1, *IL10* Hs00961622_m1, *IL12A* Hs01073447_m1, and *TGFB1* Hs00998133_m1.

Statistical Analyses. Statistical analyses were performed with Prism software (GraphPad) using the statistical tests indicated in the individual figure legends. P values of <0.05 were considered significant. All error bars represent SEM. Unless otherwise stated, three or more independent experiments were used for all assays and displayed figures are representative.

Data Availability. All study data are included in the article and supporting information.

1. P. Serra, P. Santamaria, Antigen-specific therapeutic approaches for autoimmunity. *Nat. Biotechnol.* **37**, 238–251 (2019).
2. L. Klein, E. A. Robey, C. S. Hsieh, Central $CD4^+$ T cell tolerance: deletion versus regulatory T cell differentiation. *Nat. Rev. Immunol.* **19**, 7–18 (2019).
3. D. Nemazee, Mechanisms of central tolerance for B cells. *Nat. Rev. Immunol.* **17**, 281–294 (2017).
4. S. Z. Josefowicz, L.-F. Lu, A. Y. Rudensky, Regulatory T cells: Mechanisms of differentiation and function. *Annu. Rev. Immunol.* **30**, 531–564 (2012).
5. M. G. Roncarolo, S. Gregori, R. Bacchetta, M. Battaglia, N. Gagliani, The biology of T regulatory type 1 cells and their therapeutic application in immune-mediated diseases. *Immunity* **49**, 1004–1019 (2018).
6. J. B. Wing, A. Tanaka, S. Sakaguchi, Human $FOXP3^+$ regulatory T cell heterogeneity and function in autoimmunity and cancer. *Immunity* **50**, 302–316 (2019).
7. M. Dominguez-Villar, D. A. Hafler, Regulatory T cells in autoimmune disease. *Nat. Immunol.* **19**, 665–673 (2018).
8. C. Raffin, L. T. Vo, J. A. Bluestone, T_{reg} cell-based therapies: Challenges and perspectives. *Nat. Rev. Immunol.* **20**, 158–172 (2020).
9. F. J. Quintana, D. H. Sherr, Aryl hydrocarbon receptor control of adaptive immunity. *Pharmacol. Rev.* **65**, 1148–1161 (2013).
10. C. Gutiérrez-Vázquez, F. J. Quintana, Regulation of the immune response by the aryl hydrocarbon receptor. *Immunity* **48**, 19–33 (2018).
11. V. Rothhammer, F. J. Quintana, Environmental control of autoimmune inflammation in the central nervous system. *Curr. Opin. Immunol.* **43**, 46–53 (2016).
12. L. Apetoh *et al.*, The aryl hydrocarbon receptor interacts with c-Maf to promote the differentiation of type 1 regulatory T cells induced by IL-27. *Nat. Immunol.* **11**, 854–861 (2010).
13. R. Gandhi *et al.*, Activation of the aryl hydrocarbon receptor induces human type 1 regulatory T cell-like and Foxp3(+) regulatory T cells. *Nat. Immunol.* **11**, 846–853 (2010).
14. J. A. Goettel *et al.*, AHR activation is protective against colitis driven by T cells in humanized mice. *Cell Rep.* **17**, 1318–1329 (2016).
15. F. J. Quintana *et al.*, Control of T(reg) and T(H)17 cell differentiation by the aryl hydrocarbon receptor. *Nature* **453**, 65–71 (2008).
16. F. J. Quintana *et al.*, An endogenous aryl hydrocarbon receptor ligand acts on dendritic cells and T cells to suppress experimental autoimmune encephalomyelitis. *Proc. Natl. Acad. Sci. U.S.A.* **107**, 20768–20773 (2010).
17. M. C. Takenaka *et al.*, Control of tumor-associated macrophages and T cells in glioblastoma via AHR and CD39. *Nat. Neurosci.* **22**, 729–740 (2019).
18. N. Aguilera-Montilla *et al.*, Aryl hydrocarbon receptor contributes to the MEK/ERK-dependent maintenance of the immature state of human dendritic cells. *Blood* **121**, e108–e117 (2013).
19. J. Bankoti, B. Rase, T. Simones, D. M. Shepherd, Functional and phenotypic effects of AhR activation in inflammatory dendritic cells. *Toxicol. Appl. Pharmacol.* **246**, 18–28 (2010).
20. N. T. Nguyen *et al.*, Aryl hydrocarbon receptor negatively regulates dendritic cell immunogenicity via a kynurenine-dependent mechanism. *Proc. Natl. Acad. Sci. U.S.A.* **107**, 19961–19966 (2010).
21. A. Yeste, M. Nadeau, E. J. Burns, H. L. Weiner, F. J. Quintana, Nanoparticle-mediated codelivery of myelin antigen and a tolerogenic small molecule suppresses experimental autoimmune encephalomyelitis. *Proc. Natl. Acad. Sci. U.S.A.* **109**, 11270–11275 (2012).
22. A. Yeste *et al.*, Tolerogenic nanoparticles inhibit T cell-mediated autoimmunity through SOCS2. *Sci. Signal.* **9**, ra61 (2016).

Downloaded at Palestinian Territory, occupied on November 30, 2021

www.manaraa.com

23. N. I. Kerkvliet *et al.*, Activation of aryl hydrocarbon receptor by TCDD prevents diabetes in NOD mice and increases Foxp3+ T cells in pancreatic lymph nodes. *Immunotherapy* **1**, 539–547 (2009).
24. B. Lamas *et al.*, CARD9 impacts colitis by altering gut microbiota metabolism of tryptophan into aryl hydrocarbon receptor ligands. *Nat. Med.* **22**, 598–605 (2016).
25. N. A. Hotaling, L. Tang, D. J. Irvine, J. E. Babensee, Biomaterial strategies for immunomodulation. *Annu. Rev. Biomed. Eng.* **17**, 317–349 (2015).
26. U. Bulbake, S. Doppalapudi, N. Kommineni, W. Khan, Liposomal formulations in clinical use: An updated review. *Pharmaceutics* **9**, 12 (2017).
27. L. Sercombe *et al.*, Advances and challenges of liposome assisted drug delivery. *Front. Pharmacol.* **6**, 286 (2015).
28. D. A. Anderson, 3rd, C. A. Dutertre, F. Ginhoux, K. M. Murphy, Genetic models of human and mouse dendritic cell development and function. *Nat. Rev. Immunol.*, 10.1038/s41577-020-00413-x (2020).
29. I. D. Mascanfroni *et al.*, IL-27 acts on DCs to suppress the T cell response and autoimmunity by inducing expression of the immunoregulatory molecule CD39. *Nat. Immunol.* **14**, 1054–1063 (2013).
30. F. J. Quintana, A. Yeste, I. D. Mascanfroni, Role and therapeutic value of dendritic cells in central nervous system autoimmunity. *Cell Death Differ.* **22**, 215–224 (2015).
31. M. C. Takenaka, F. J. Quintana, Tolerogenic dendritic cells. *Semin. Immunopathol.* **39**, 113–120 (2017).
32. S. Kress, W. F. Greenlee, Cell-specific regulation of human CYP1A1 and CYP1B1 genes. *Cancer Res.* **57**, 1264–1269 (1997).
33. J. Song *et al.*, A ligand for the aryl hydrocarbon receptor isolated from lung. *Proc. Natl. Acad. Sci. U.S.A.* **99**, 14694–14699 (2002).
34. J. Kaye *et al.*, Laquinimod arrests experimental autoimmune encephalomyelitis by activating the aryl hydrocarbon receptor. *Proc. Natl. Acad. Sci. U.S.A.* **113**, E6145–E6152 (2016).
35. U. Grohmann, F. Fallarino, P. Puccetti, Tolerance, DCs and tryptophan: Much ado about IDO. *Trends Immunol.* **24**, 242–248 (2003).
36. M. S. Denison, A. A. Soshilov, G. He, D. E. DeGroot, B. Zhao, Exactly the same but different: Promiscuity and diversity in the molecular mechanisms of action of the aryl hydrocarbon (dioxin) receptor. *Toxicol. Sci.* **124**, 1–22 (2011).
37. I. D. Mascanfroni *et al.*, Metabolic control of type 1 regulatory T cell differentiation by AHR and HIF1-α. *Nat. Med.* **21**, 638–646 (2015).
38. S. Batzri, E. D. Korn, Single bilayer liposomes prepared without sonication. *Biochim. Biophys. Acta* **298**, 1015–1019 (1973).
39. R. Bazzi, T. D. Bradshaw, J. C. Rowlands, M. F. G. Stevens, D. R. Bell, 2-(4-Amino-3-methylphenyl)-5-fluorobenzothiazole is a ligand and shows species-specific partial agonism of the aryl hydrocarbon receptor. *Toxicol. Appl. Pharmacol.* **237**, 102–110 (2009).
40. E. C. Henry, T. A. Gasiewicz, Molecular determinants of species-specific agonist and antagonist activity of a substituted flavone towards the aryl hydrocarbon receptor. *Arch. Biochem. Biophys.* **472**, 77–88 (2008).
41. V. Rothhammer *et al.*, Detection of aryl hydrocarbon receptor agonists in human samples. *Sci. Rep.* **8**, 4970 (2018).
42. E. Hauben *et al.*, Activation of the aryl hydrocarbon receptor promotes allograft-specific tolerance through direct and dendritic cell-mediated effects on regulatory T cells. *Blood* **112**, 1214–1222 (2008).
43. J. D. Mezrich *et al.*, An interaction between kynurenine and the aryl hydrocarbon receptor can generate regulatory T cells. *J. Immunol.* **185**, 3190–3198 (2010).
44. E. Bettelli *et al.*, Myelin oligodendrocyte glycoprotein-specific T cell receptor transgenic mice develop spontaneous autoimmune optic neuritis. *J. Exp. Med.* **197**, 1073–1081 (2003).
45. E. Claassen, Post-formation fluorescent labelling of liposomal membranes. In vivo detection, localisation and kinetics. *J. Immunol. Methods* **147**, 231–240 (1992).
46. T. Korn *et al.*, Myelin-specific regulatory T cells accumulate in the CNS but fail to control autoimmune inflammation. *Nat. Med.* **13**, 423–431 (2007).
47. P. V. Lehmann, T. Forsthuber, A. Miller, E. E. Sercarz, Spreading of T-cell autoimmunity to cryptic determinants of an autoantigen. *Nature* **358**, 155–157 (1992).
48. C. L. Vanderlugt, S. D. Miller, Epitope spreading in immune-mediated diseases: Implications for immunotherapy. *Nat. Rev. Immunol.* **2**, 85–95 (2002).
49. L. Mayo *et al.*, Regulation of astrocyte activation by glycolipids drives chronic CNS inflammation. *Nat. Med.* **20**, 1147–1156 (2014).
50. V. Rothhammer *et al.*, Sphingosine 1-phosphate receptor modulation suppresses pathogenic astrocyte activation and chronic progressive CNS inflammation. *Proc. Natl. Acad. Sci. U.S.A.* **114**, 2012–2017 (2017).
51. L. Mayo *et al.*, IL-10-dependent Tr1 cells attenuate astrocyte activation and ameliorate chronic central nervous system inflammation. *Brain* **139**, 1939–1957 (2016).
52. B. Bielekova *et al.*, Encephalitogenic potential of the myelin basic protein peptide (amino acids 83-99) in multiple sclerosis: Results of a phase II clinical trial with an altered peptide ligand. *Nat. Med.* **6**, 1167–1175 (2000).
53. H. Garren *et al.*; BHT-3009 Study Group, Phase 2 trial of a DNA vaccine encoding myelin basic protein for multiple sclerosis. *Ann. Neurol.* **63**, 611–620 (2008).
54. D. R. Getts *et al.*, Microparticles bearing encephalitogenic peptides induce T-cell tolerance and ameliorate experimental autoimmune encephalomyelitis. *Nat. Biotechnol.* **30**, 1217–1224 (2012).
55. M. Juryńczyk *et al.*, Immune regulation of multiple sclerosis by transdermally applied myelin peptides. *Ann. Neurol.* **68**, 593–601 (2010).
56. A. Lutterotti *et al.*, Antigen-specific tolerance by autologous myelin peptide-coupled cells: A phase 1 trial in multiple sclerosis. *Sci. Transl. Med.* **5**, 188ra75 (2013).
57. F. J. Quintana, P. Carmi, F. Mor, I. R. Cohen, Inhibition of adjuvant arthritis by a DNA vaccine encoding human heat shock protein 60. *J. Immunol.* **169**, 3422–3428 (2002).
58. S. Tsai *et al.*, Reversal of autoimmunity by boosting memory-like autoregulatory T cells. *Immunity* **32**, 568–580 (2010).
59. H. L. Weiner, A. P. da Cunha, F. Quintana, H. Wu, Oral tolerance. *Immunol. Rev.* **241**, 241–259 (2011).
60. A. Carambia *et al.*, Nanoparticle-based autoantigen delivery to Treg-inducing liver sinusoidal endothelial cells enables control of autoimmunity in mice. *J. Hepatol.* **62**, 1349–1356 (2015).
61. R. A. Maldonado *et al.*, Polymeric synthetic nanoparticles for the induction of antigen-specific immunological tolerance. *Proc. Natl. Acad. Sci. U.S.A.* **112**, E156–E165 (2015).
62. D. Gonzalez-Carter *et al.*, Targeting nanoparticles to the brain by exploiting the blood-brain barrier impermeability to selectively label the brain endothelium. *Proc. Natl. Acad. Sci. U.S.A.* **117**, 19141–19150 (2020).
63. A. Awasthi *et al.*, A dominant function for interleukin 27 in generating interleukin 10-producing anti-inflammatory T cells. *Nat. Immunol.* **8**, 1380–1389 (2007).
64. M. Ito *et al.*, Brain regulatory T cells suppress astrogliosis and potentiate neurological recovery. *Nature* **565**, 246–250 (2019).
65. J. L. Kanter *et al.*, Lipid microarrays identify key mediators of autoimmune brain inflammation. *Nat. Med.* **12**, 138–143 (2006).
66. F. J. Quintana *et al.*, Antigen microarrays identify CNS-produced autoantibodies in RRMS. *Neurology* **78**, 532–539 (2012).
67. F. J. Quintana *et al.*, Antigen microarrays identify unique serum autoantibody signatures in clinical and pathologic subtypes of multiple sclerosis. *Proc. Natl. Acad. Sci. U.S.A.* **105**, 18889–18894 (2008).
68. F. J. Quintana *et al.*, Functional immunomics: Microarray analysis of IgG autoantibody repertoires predicts the future response of mice to induced diabetes. *Proc. Natl. Acad. Sci. U.S.A.* **101** (suppl. 2), 14615–14621 (2004).
69. F. J. Quintana *et al.*; Canadian Pediatric Demyelinating Disease Network, Epitope spreading as an early pathogenic event in pediatric multiple sclerosis. *Neurology* **83**, 2219–2226 (2014).
70. W. H. Robinson *et al.*, Autoantigen microarrays for multiplex characterization of autoantibody responses. *Nat. Med.* **8**, 295–301 (2002).
71. T. M. Allen, P. R. Cullis, Liposomal drug delivery systems: From concept to clinical applications. *Adv. Drug Deliv. Rev.* **65**, 36–48 (2013).
72. V. Rothhammer *et al.*, Type I interferons and microbial metabolites of tryptophan modulate astrocyte activity and central nervous system inflammation via the aryl hydrocarbon receptor. *Nat. Med.* **22**, 586–597 (2016).
73. N. L. Bray, H. Pimentel, P. Melsted, L. Pachter, Near-optimal probabilistic RNA-seq quantification. *Nat. Biotechnol.* **34**, 525–527 (2016).
74. B. Li, C. N. Dewey, RSEM: Accurate transcript quantification from RNA-seq data with or without a reference genome. *BMC Bioinformatics* **12**, 323 (2011).
75. A. Zhu, J. G. Ibrahim, M. I. Love, Heavy-tailed prior distributions for sequence count data: Removing the noise and preserving large differences. *Bioinformatics* **35**, 2084–2092 (2019).
76. N. Leng *et al.*, EBSeq-HMM: A bayesian approach for identifying gene-expression changes in ordered RNA-seq experiments. *Bioinformatics* **31**, 2614–2622 (2015).

Downloaded at Palestinian Territory, occupied on November 30, 2021

www.manaraa.com